ELSEVIER

Chemical Geology 190 (2002) 303–319

CHEMICAL GEOLOGY
INCLUDING
ISOTOPE GEOSCIENCE

www.elsevier.com/locate/chemgeo

Natural attenuation of TCE, As, Hg linked to the heterogeneous oxidation of Fe(II): an AFM study

Laurent Charlet[a,*], Dirk Bosbach[b,1], Tanya Peretyashko[a,2]

[a] *Environmental Geochemistry Group LGIT, Observatory of Earth and Planetary Sciences (OSUG), University of Grenoble-I/CNRS, BP 53, F-38041 Grenoble, France*
[b] *Institut für Mineralogie, Universität Münster, Corrensstr. 24, D-48149 Münster, Germany*

Abstract

Hydrous ferric oxide (HFO) colloids formed, in strictly anoxic conditions upon oxidation of Fe^{2+} ions adsorbed on mineral surface, were investigated under in situ conditions by contact mode atomic force microscopy (AFM). Freshly cleaved and acid-etched large single crystals of near endmember phlogopite were pre-equilibrated with dissolved Fe(II) and then reacted with Hg(II), As(V) and trichlorethene (TCE)-bearing solutions at 25 °C and 1 atm. HFO structures are found to be of nanometer scale. The As(V)–Fe(II) and Hg(II)–Fe(II) reaction products are round (25 nm) microcrystallites located predominantly on the layer edges and are indicative of an accelerated Fe(II) oxidation rate upon formation of Fe(II) inner sphere surface complexes with the phyllosilicate edge surface sites. On the other hand, TCE–Fe(II)–phlogopite reaction products are needle-shaped (45 nm long) particles located on the basal plane along the Periodic Bond Chains (PCBs) directions. Experiments with additions of sodium chloride confirm the importance of the Fe(II) adsorption step in the control of the overall heterogeneous Fe(II)–TCE electron transfer reaction.

Kinetic measurements at the nanomolar level of Hg° formed upon reduction of Hg(II) by Fe(II) in presence of phlogopite particles provide further convincing evidence for reduction of $Hg(II)_{aq}$ coupled to the oxidation of Fe(II) adsorbed at the phlogopite–fluid interface, and indicate that sorption of Fe(II) to mineral surfaces enhances the reduction rate of Hg(II) species. The Hg(II) reduction reaction follows a first-order kinetic law. Under our experimental conditions, which were representative of many natural systems, 80% of the mercury is transferred to the atmosphere as Hg° in less than 2 h.

The reduction of a heavy metal (Hg), a toxic oxyanion (arsenate ion) and a chlorinated solvent (TCE) thus appear to be driven by the high reactivity of adsorbed Fe(II). This is of environmental relevance since these three priority pollutants are that way reductively transformed to a volatile, an immobilizable and a biodegradable species, respectively. Such kinetic data and reaction pathways are important in the evaluation of natural evaluation scenarios, in the optimization of Fe(II)/mineral mixtures as reductants in technical systems, and in general, in predicting the fate and transport of pollutants in natural systems.

Keywords: Ferrous iron; Natural attenuation; Clay edges; Mercury; AFM

* Corresponding author. Tel.: +33-4-7862-8020; fax: +33-4-76828101.
E-mail address: laurent.charlet@obs.ujf-grenoble.fr (L. Charlet).
[1] Present address: Forschungszentrum Karlsruhe, Institut für Nukleare Entsorgung, Postfach 3640, 76021 Karlsruhe, Germany.
[2] Present address: Department ESPN, Berkeley, CA 94720-3110, USA.

0009-2541/02/$ - see front matter © 2002 Published by Elsevier Science B.V.
PII: S0009-2541(02)00122-5

1. Introduction

Ferrous iron has been shown to provide an effective means for removing a variety of pollutant including nitrite, nitrate, chromium, selenate, uranium, vanadate, pertechnetate, and nitrobenzene from aqueous solution (Schwertmann and Pfab, 1994; Klausen et al., 1995; Cui and Eriksen, 1996; Ottley et al., 1997; Myrreni et al., 1997; Buerge and Hug, 1999; Liger et al., 1999). A common feature of these reductive transformation reactions by ferrous iron is that sorbed ferrous iron is always much more reactive than dissolved iron(II) present in the background electrolyte solution. Indeed, rates of homogeneous reduction by dissolved Fe(II) are exceedingly slow. Surface Fe(II) complexes formed with hydrous iron oxides, silicates and sulfides, are on the other hand very efficient reductants from a thermodynamic (Fig. 1) as well as from a kinetic point of view (Stumm and Sulzberger, 1992).

The reductive transformation of an oxidized species ox by surface Fe(II) may be written as:

$$n(\mathrm{Fe^{II}})_{\mathrm{sorbed}} + \mathrm{ox} = n\mathrm{Fe(OH)_3(s)} + \mathrm{red} \qquad (1)$$

where n is the number of electrons that must be transferred to ox in order to produce red (e.g. n=2, 3 and 6 for U(VI), Cr(VI) and nitrobenzene, respectively). However, the reaction rate is not a direct function of the total sorbed Fe(II) concentration. Instead, it has been shown by Charlet et al. (1998b) to be proportional to the concentration of the >FeOFe^{II}OH° hydroxylated surface complex of Fe(II), a complex formed with one surface functional group >FeOH°, one Fe^{2+} ion and

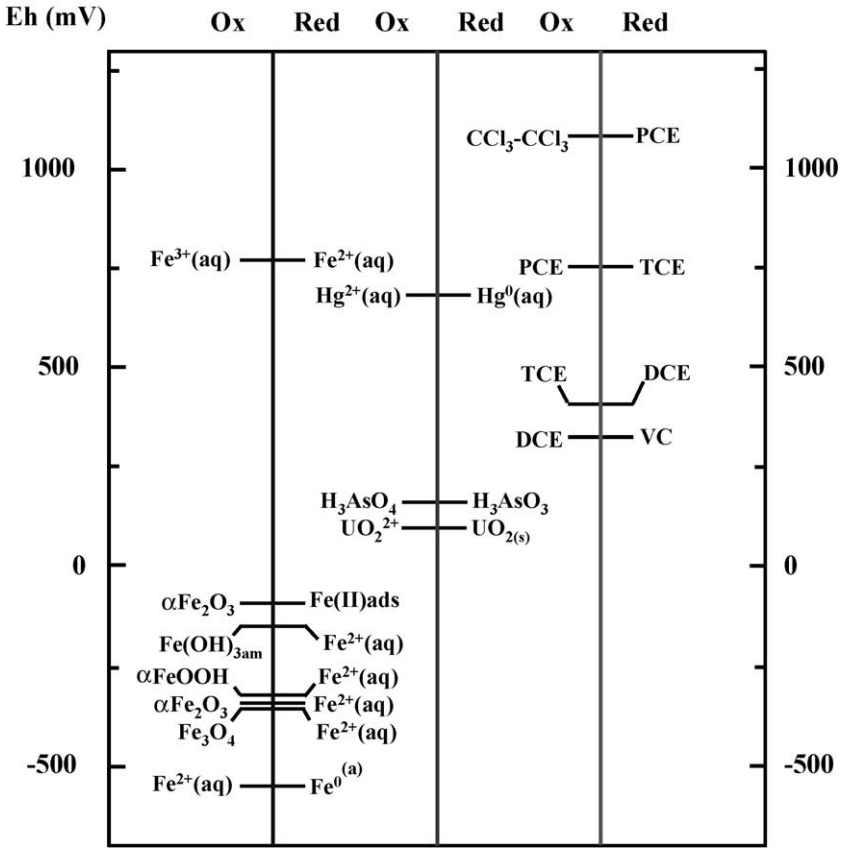

Fig. 1. E_h values computed for various Fe(II)/Fe(III) couples (adapted from Stumm and Sulzberger, 1992) and for TCE/DCE, As(V)/As(III) and Hg(II)/Hg° at pH 7.0.

two hydroxyl ions. Reaction (1) has been also shown to follow a second-order rate law (Charlet et al., 1998a; Buerge and Hug, 1999; Liger et al., 1999), and the observed rate to be a function of $>FeOFe^{II}OH^{\circ}$ as well as oxidant concentration according to:

$$-\frac{d[Ox]}{dt} = k[>FeOFe^{II}OH^{\circ}][Ox] \quad \text{with}$$
$$Ox = U(VI), Cr(VI) \text{or } ArNO_2 \qquad (2)$$

Eq. (2) indicates that, among the electrons transferred in reaction (1), only the first electron transfer is rate limiting (Charlet et al., 1998a).

The reduction mechanism outlined in Eqs. (1) and (2) can be further compared to the homogeneous oxidation of Fe(II) by oxygen. The oxygenation is routinely used in a number of European countries in in situ iron removal procedures (Appelo et al., 2000). Electron transfer takes place between the dissolved oxygen present in injection water and the dissolved Fe(II) species originally present in ground water. Both dissolved OH^- (aq) and surface hydroxyl groups facilitate the electron transfer to O_2, as the OH^- ligands donate electron density to Fe(II) through both σ and π systems, which results in metal basicity and increased reducing power (Luther, 1990). Above pH 5.0, the homogeneous oxygenation of Fe(II) in solution follows a rate law (Stumm and Sulzberger, 1992) similar to Eq. (2):

$$-\frac{d[Fe(II)]}{dt} = k[Fe(OH)_2^{\circ}]P_{O_2} \qquad (3)$$

In comparison to oxidation in homogeneous solution, sorption of Fe(II) to mineral surfaces enhances the oxygenation of sorbed Fe(II) species. This has been demonstrated for Fe(II) present on Fe-oxyhydroxide surfaces (Tamura et al., 1980) as well as on clay mineral surfaces. This reaction can lead to autocatalytic processes. Upon oxidation of a Fe(II) surface species, Fe-oxyhydroxide precipitates. As a consequence of the formation of a new phase, new mineral surface area is generated, which serves as a substrate for further Fe(II) sorption. Therefore, as the reaction proceeds, the heterogeneous precipitation of Fe-oxyhydroxides leads to the formation of new sites for Fe(II) sorption, and the reaction rate speeds up. After the initial injection of a defined volume of oxygenated water, subsequently larger volumes of ground water can then be pumped with a lower iron concentration than is found in native ground water (Appelo et al., 2000).

Natural attenuation is defined by EPA (1997) as "a variety of processes that act without human intervention to reduce the toxicity, mobility and concentration of contaminants in soils or groundwater". Surface Fe(II) is shown by the abovementioned studies to be a natural mean to remove priority compounds from groundwater and its efficiency may be compared to that of Fe°, which has been used in engineered barriers to remove Cr(VI), U(VI) and chlorinated solvent from contaminated groundwater (Orth and Gillham, 1996). This efficiency of surface Fe(II) has been verified in a number of field studies. For instance, in aquifers located below a source of organic carbon, e.g. below a waste dumping site, the organic matter input induces the formation of a large Fe reduction zone, where only 2% of the total Fe(II) is present as dissolved Fe(II), up to 20% is present as exchangeable sorbed Fe(II), the remainder being in a solid form (pyrite and "AVS") (Heron and Christensen, 1995). Sorbed Fe(II) is very effective in aquifers to remove nitrate (Ernstsen, 1996; Vanek, 1990), nitrite (Sorensen and Thorling, 1991) and chlorinated aliphatics (Christensen et al., 1994) from groundwater. This has important consequences for strategies to improve ground water quality in such environments.

Macroscopic experimental approaches, where the fluid composition during experiments is monitored, have provided detailed information about the heterogeneous oxidation of Fe(II) surface species. However, the actual reactive sites and products of reaction (1) have not yet been identified simultaneously and unambiguously. Atomic force microscopy (AFM) has proven to be a powerful technique for the characterization of clay mineral surface microtopography (Bickmore et al., 1999a,b) and the identification of reactive surface area (Rufe and Hochella, 1999; Bosbach et al., 2000) at molecular scales. One of the greatest strengths of AFM is that it can characterize surface microtopography directly in solutions so it can track in situ and in real time the dissolution of clay minerals (Bosbach et al., 2000; Bickmore et al., 2001), the adsorption of small polymers or humic acids on a flat mineral surfaces

(Plaschke et al., 1999; Eggleston and Stumm, 1993), or the oxygenation of dissolved Fe(II) and subsequent crystal growth of (100) and (110) faces of goethite (Weidler et al., 1998; Hug et al., 1997).

In this study, we expand upon the oxygenation experiments described above to further test the hypothesis that in the presence of $[Fe(II)]_i$=10–250 μM, the Fe(II) oxidation by various priority pollutants occurs primarily through heterogeneous reactions at the clay mineral/water interface. The initial Fe(II) concentration range was chosen for three reasons: (i) Buerge and Hug (1999) have shown that at $[Fe(II)]_i 2.5\times10^{-4}$ M, the reaction would become too rapid for in situ imaging with AFM. (ii) At lower initial Fe(II) concentrations, reaction products would be too sparse to be detected even by a high-resolution microscopic technique, such as AFM. (iii) The chosen Fe(II) concentration window represents the ferrous iron concentration of many reducing natural environments, such as aquifers (McArthur et al., 2000), lake hypolimnion (Cossa et al., 1994) and sediments (Davison et al., 1991). Although in nature, oxygen, nitrate and manganese oxides are often the most abundant electron acceptors, we chose to use Hg, As and trichlorethene (trichlorethylene or TCE) because their reduction by surface Fe(II) leads to products belonging to three different thermodynamic phases, i.e. to gas ($Hg^{\circ}(g)$), solid ($Fe(OH)_3(s)$ coprecipitated with As) and liquid (DCE(aq)) phases, respectively. The ferric (hydr)oxide phase formed in the course of the reaction at the phlogopite/water interface may therefore be drastically different.

2. Materials and methods

2.1. Materials

Large phlogopite single crystals, several centimeters in diameter and up to 2 mm in thickness, were provided by the Mineral Museum of the University of Münster. Phlogopite—$(K,Na)_{x-y}((Mg^{2+}, Fe^{2+})_{3-y}(Fe^{3+})_y)(Si_{4-x}Al_x)O_{10}(OH)_2$—as a trioctahedral mica contains Mg as the dominating cation in the octahedral sites. Only minor amounts of Fe(II) and Fe(III) are present. Since it has a perfect cleavage parallel to (001), single crystals were cleaved by using a scotch tape. Freshly cleaved phlogopite surfaces consist of large atomically flat terraces. The occurrence of molecular steps is rare. In order to study reaction at layer broken edges, we have induced the formation of etch pits and consequently the formation of molecular steps by the following procedure. A small (36 mm^2) square of a freshly cleaved phlogopite sample was etched for 2 min in concentrated distilled HF at room temperature and rinsed with a stream of deionized water.

Iron (II), Arsenic(V) and mercury(II) stock solutions at concentrations of 10^{-3} M Fe(II), 5×10^{-4} M As(V) and 10^{-2} M Hg(II) were prepared from $FeSO_4\times7H_2O$ (Merck), $Na_2HAsO_4\times7H_2O$ (Fluka) and $HgCl_2$ (J.T. Baker), using boiled and degassed Milli-Q deionized water (BDDIW), acidified with ultrapure HNO_3. The 1 g l^{-1} TCE stock solution was made in two steps. First, a known weight of TCE is dissolved in methanol, second an aliquot of this solution is dissolved in BDDIW to 5×10^{-3} M TCE. The ionic strength was adjusted with a 1 M NaCl solution. The pH in our experiments was controlled by reagent grade MOPS buffer (Fisher Scientific). MOPS solution (0.1 M) was titrated to pH 7.5 with reagent grade NaOH solution.

2.2. Macroscopic kinetic experiments

Sixty micrograms of ground phlogopite was added to 150 ml of deoxygenated water and 29 ml of buffer in a 200 ml titration reactor. Ferrous sulfate was added to obtain a 1.0 10^{-5} M Fe(II) initial concentration. The initial pH of the suspension was 7.5. The reactor was purged continuously with ultrapure Ar to avoid oxidation of Fe(II) to Fe(III) by ultratraces of oxygen. The suspension was equilibrated for 24 h. A 50 ml aliquot was then transferred to a 125 ml Teflon bubbler, and mixed at $t=0$ with an aliquot of a 0.25 μg l^{-1} stock Hg(II) solution, to get a 50 pM initial Hg(II) concentration in the suspension. This very low concentration is representative (and even larger) than most Hg(II) dissolved concentrations found in polluted surface waters (e.g. Cossa et al., 1994). At fixed time intervals, produced gaseous mercury was purged with ultra pure Ar, stored onto gold trap, and determined by cold vapor atomic fluorescence spectroscopy (CVAFS) using Tekran detector (Bloom and Fitzgerald, 1988). The stand-

ard deviation of the bubbler blank was on average 1.4 pg resulting in detection limit (3xSTD of blanks) of 4.2 pg.

2.3. Atomic force microscopy (AFM)

The small (36 mm^2) square of a freshly cleaved phlogopite was introduced in a vial, together with aliquots of the iron(II), oxidant (As, Hg or TCE) and MOPS stock solutions. The total concentration was equal to 2.5×10^{-4} M for Fe(II), 5×10^{-4} M for As(V) and 10^{-3} M for TCE. In the case of Hg(II) experiment, the total concentration was equal to 1×10^{-5} M for Fe(II) and 3×10^{-5} M for Hg(II). In order to be able to observe reaction (1) solid products, a high Hg(II) total concentration had to be used, which is 10^3 higher than the concentration used in the kinetic experiment. Total volume was equal to 10 ml. The solution was flushed with argon before closing the vial tightly. Further, in order to ensure that no oxygen could access the solution, the vial was wrapped with teflon tape. The vials were shaken and then stored in an evacuated dessicator. Some samples had their ionic strength set up equal to 0.1 M NaCl. Reaction time ranged from 30 min to 5 days.

After the desired reaction time, the phlogopite slides were removed with Teflon tweezers, gently flushed with a stream of BDDIW for 5 min, and oven dried at 45 °C for 10 min. It was then mounted with double-sided sticky tape to the AFM sample holder.

We have used a Digital Instruments Nanoscope III AFM. Images were taken in air in contact mode (CM) as well as in tapping mode (TM). Oxide sharpened Si_3N_4 Twin tips (Digital Instruments) Cantilevers with integrated pyramidal Twin Tips and with a force constant of 0.12 N/m were used for CM measurements and etched Si probes (Olympus) with a force constant of about 40 N/m and a resonance frequency of about 300 kHz were used for TM measurements. All images shown in this paper were taken in contact mode. Although tapping mode ensures significantly lower tip-sample loading forces, we obtained significantly better images in contact mode. Particle diameter and height data were obtained independently using the Digital Instruments software.

3. Results

3.1. Reduction of Hg(II) by Fe(II) in the presence of phlogopite

Fig. 2a shows a typical example of the reactivity of a system containing Hg(II) at pH 7.5 in aqueous Fe(II) solutions with and without suspended phlogopite. There is virtually no change in the Hg(II) oxidation state in pure 10 mM Fe(II) solution (without suspended phlogopite). There is also no Hg(II) reduction

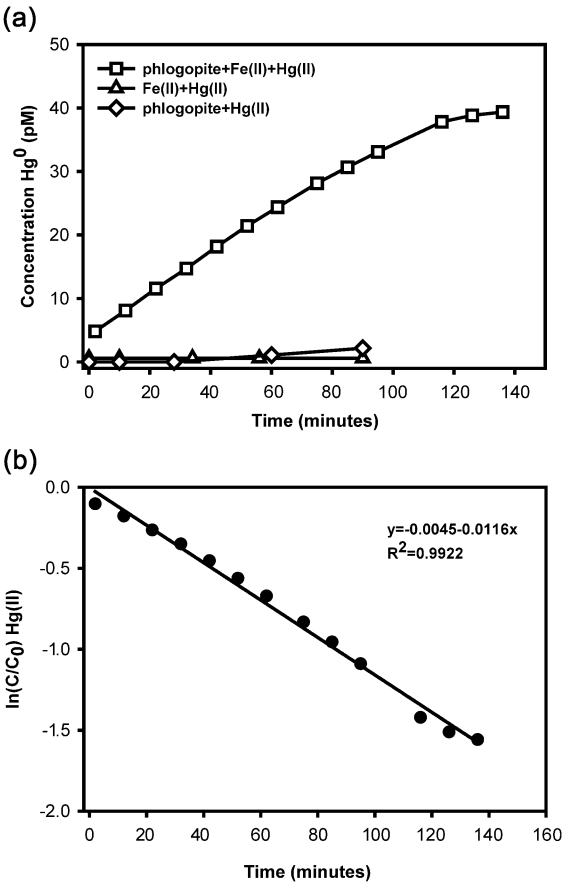

Fig. 2. In situ measurement of Hg° production by an aqueous solution containing 10 μM Fe(II), 50 pM Hg(II), 0.015 M MOPS and 3 mg l^{-1} phlogopite at pH 7.5. (a) □—suspension of phlogopite with Fe(II) and Hg(II), △—solution of Fe(II) and Hg(II) without phlogopite, ◇—suspension of phlogopite with Hg(II). (b) Natural logarithm of the relative concentration (C/C_0) for Hg(II) vs. time. Solid line is the linear regression through the data.

in pure phlogopite suspension (without additional Fe(II)), although the reduction of Hg(II) with minerals containing traces of Fe(II) is thermodynamically possible at neutral pH (Fig. 1). Therefore, either there is not enough Fe(II) present in our phlogopite sample or the reduction of Hg(II) with reduced electron donors that may be part of the phlogopite lattice—or which are present in solution—is a rather slow process.

However, in suspensions of phlogopite that also contain additional Fe(II), significant amounts of Hg(II) become reduced. Clearly, the adsorption of Fe(II) to the phlogopite surface creates highly reactive sites for the reduction of Hg(II). During the entire length of the experiments (140 min), i.e. up to the disappearance of nearly 80% of initial mercury from solution, the formation of Hg° follows an apparent first-order kinetic law (Fig. 2b):

$$\ln\left(\frac{[\mathrm{Hg(II)}]_t}{[\mathrm{Hg(II)}]_0}\right) = -k_{\mathrm{obs}}t \qquad (4)$$

where $[Hg(II)]_t$ and $[Hg(II)]_0$ are the Hg(II) concentrations at time t and time 0, respectively, and k_{obs} is the observed pseudo-first-order rate constant under the prevalent conditions. The pseudo-first-order rate constant value is equal to 0.0116 min^{-1}, and the half time of Hg(II) in the suspension is 58 min.

With respect to natural situations, this attenuation mechanism is remarkably efficient. Although the Fe(II) and phlogopite concentrations were rather low (10 μM and 3 mg l^{-1}, respectively), 80% of the mercury could be transformed from an aqueous species (predominantly $Hg(OH)_2^{\circ}(aq)$) to a gaseous species ($Hg^{\circ}(g)$) and be subsequently transferred to the atmosphere within 2 h. Therefore, clay minerals do not act only as a storage facility for contaminants; they serve also as a template for heterogeneous decontamination reactions. This is especially important since mercury present in anoxic environment may otherwise be microbiologically transformed to methyl mercury, which is much more toxic and bioaccumulate in the trophic chain.

3.2. AFM observation of unreacted phlogopite (001)

In order to characterize the reactivity of phlogopite surfaces and to identify reactive sites for the heterogeneous oxidation of adsorbed Fe(II), we have treated freshly cleaved phlogopite with HF. Up to 10^9 cm^{-2} etch pits formed on the (001) basal surface upon HF treatment (Fig. 3a). The depth of the etch pits was up to five molecular TOT layers. However, etch pits with a depth of one TOT layer (=10.2 Å) were by far the most abundant ones. The etch pit morphology is defined by step edges parallel to <100> and <110> (Fig. 3b), which one would expect for a mica (001) surface according to PBC theory (Hartman, 1983; White and Zelazny, 1988). The dissolution rate of the step edges in pure water at pH 7.5 is small. Rufe and Hochella (1999) found that the retreat velocity of molecular steps on a phlogopite (001) surface at pH 6 is $4 \cdot 10^{-5}$ nm/s. Therefore, within the time frame of our experiments, there will be no change in microtopography on our samples.

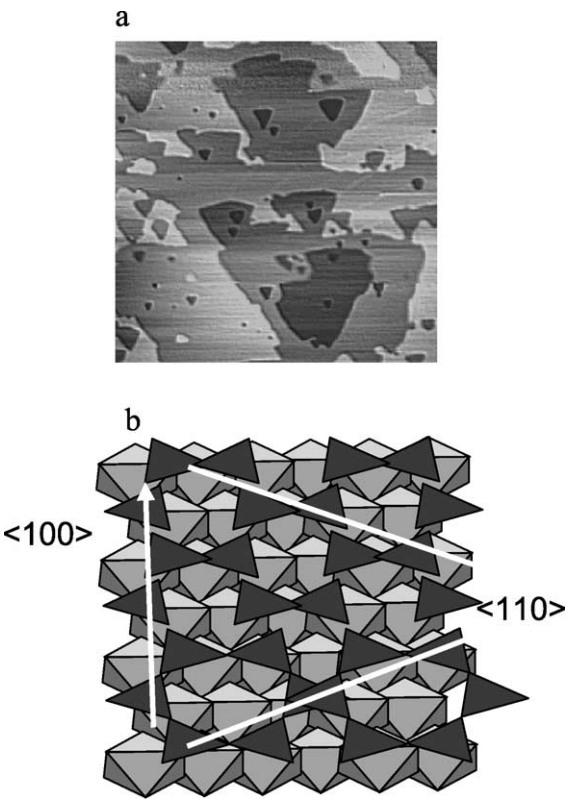

Fig. 3. In situ AFM images of the surface of unreacted phlogopite (a) and Periodic Bond Chains (PCBs) directions at phlogopite surface (b). Different shades of grey represent different (001) terraces; the darker, the deeper.

The microtopography generated by HF treatment turned out to be a suitable substrate for the characterization of the reactivity of the basal surface as well as step edges, which represent {hk0} crystal faces.

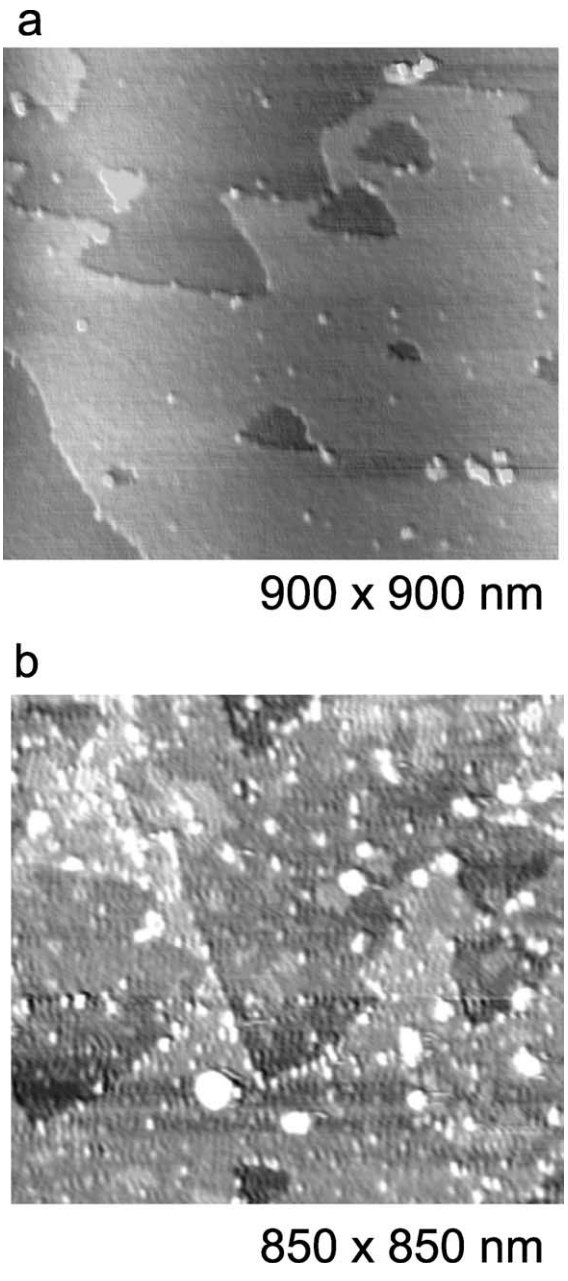

Fig. 4. In situ AFM images of the phlogopite surface reacted with Fe(II) and mercury 20 h (a) and 59 h (b) after injecting the Hg(II) solution. (Scan size=900 μm (a) and 850 μm (b) on a side, respectively).

3.3. AFM observation of Hg(II) reacted phlogopite (001)

After reacting a phlogopite single crystal with a Fe(II) solution, no changes in microtopography can be identified, indicating that no precipitation of, e.g. Fe-(hydr)oxide occurred. This observation agrees with our macroscopic experiments.

However, after adding Hg(II) to the Fe(II) solution with phlogopite single crystal, we found significant changes in microtopography (Fig. 4b). Although the etch pits, which where generated by HF treatment can still be recognized, small 25 nm wide microprecipitates of presumably Fe-(hydr)oxide have formed (Table 1). Nuclei appeared on the (001) surface after approximately 1 h and remained to the end of the experiment. Unfortunately, no reliable data were obtained during the experiment for the changes of the length in the direction of the *c*-axis of the crystal.

3.4. AFM observation of As(V) reacted phlogopite sample

Fig. 5 shows AFM images of iron (hydr)oxide particles formed on a HF treated phlogopite (001) surface after various reaction times of As(V) with the phlogopite previously equilibrated with Fe(II). Although some nuclei are found at random on the (001) face of phlogopite after 30 min, the distribution

Table 1
Dimensions of Fe microprecipitates as measured with AFM

Oxidant, reaction time	Length (nm)	Width (nm)	Height (nm)
Hg, 20 h	29.4±2.7	29.4±2.7	2.8±1.0
Hg, 59 h	22.7±6.0	22.7±6.0	2.8±0.6
As, 30 min	23.8±3.2	23.8±3.2	1.6±0.9
As, 6 days	31.2±8.5	31.2±8.5	3.5±1.6
As, 6 days	22.4±2.4	22.4±2.4	3.0±0.3
TCE, 1 day	43.1±6.2	43.1±6.2	1.9±1.5
TCE, 5 days (no NaCl)	52.1±3.9	22.9±3.1	3.5±0.3

The width and length are almost identical (except for TCE, 5 days, no NaCl), indicating a circular or spherical morphology. The standard deviation given for every sample is based on 5–20 individual measurements.

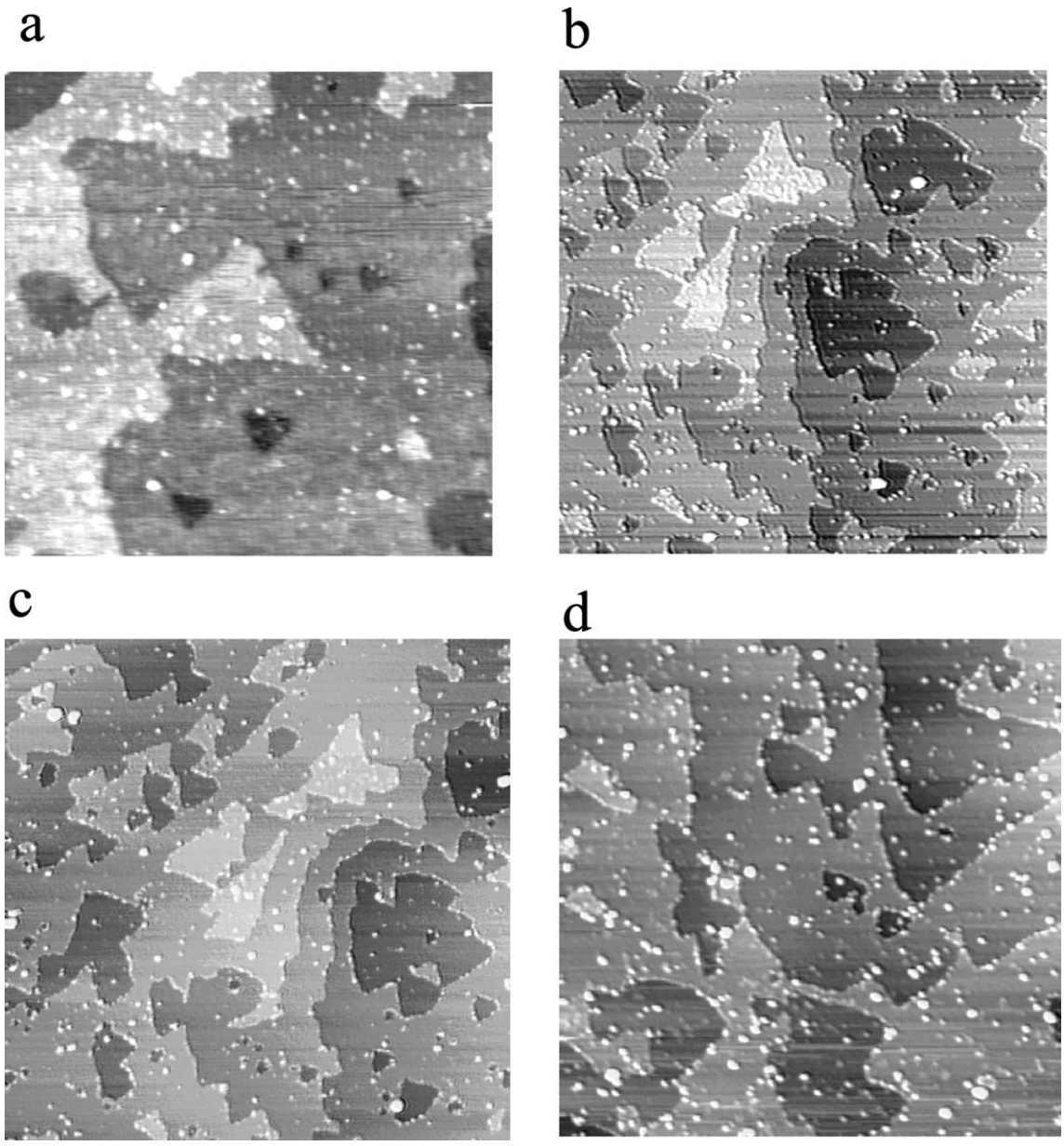

Fig. 5. In situ AFM images of the phlogopite surface reacted with Fe(II) and As(V) with no background ionic medium. Reaction time: 30 min (a), 2 h (b), and 6 days (c and d). Scanned surface sides are 0.9, 1.4, 1.6 and 1 μm, respectively.

of particles start to be well organized after 2 h reaction time. Later on, the size of the globular nuclei does not change with time and remains closed to 24 nm (Table 1). Fig. 6 depicts how the width, length and height reported in Table 1 for these microcrystallites are recorded.

With time, more and more of these nanoparticles are formed along the walls of the etch pits, while the particle density on the (001) phlogopite plane remained constant. This behavior is clearly illustrated in Fig. 5, which is a time series of AFM images taken during the precipitation of iron

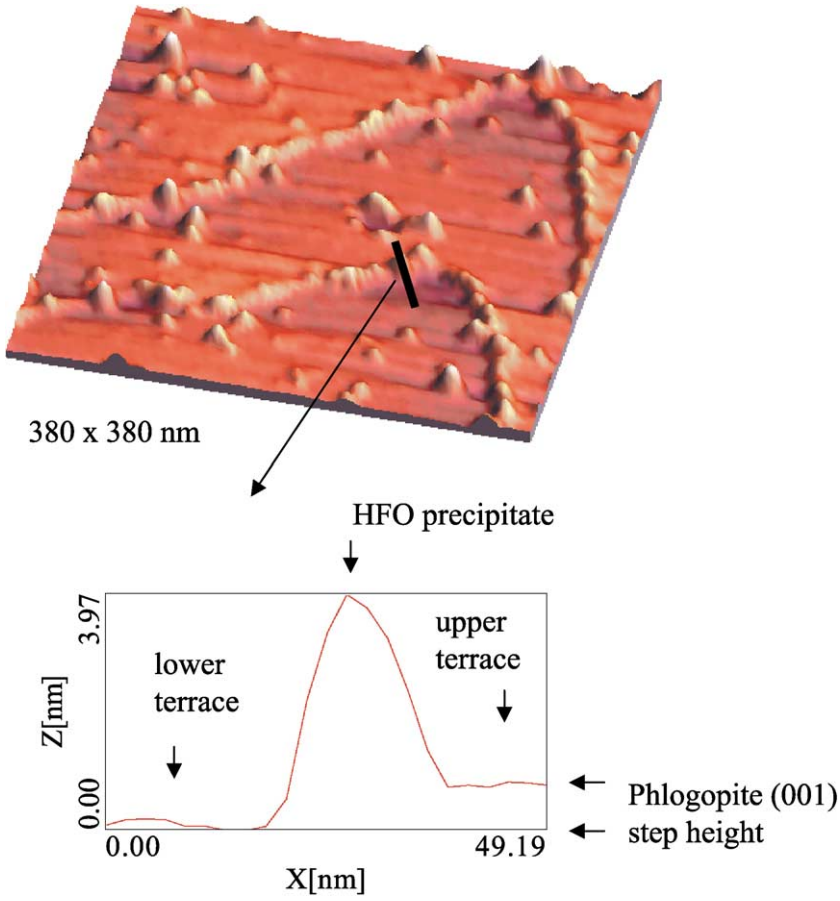

Fig. 6. Zoom (a) and transect (b) of the AFM image of the Fe(II)-phlogopite surface reacted 6 days with As(V).

(hydr)oxide crystallites in pH 7.5 solution. The reaction fronts at broken edges appear to offer very reactive defect sites.

4. AFM observation of TCE reacted phlogopite sample

Ferric hydrous oxides formed at the phlogopite surface upon oxidation of surface Fe(II) by TCE are shown in Fig. 7a,b. In the presence of high background ionic strength, nearly no particles are formed (Fig. 7c,d). This demonstrates that Fe(II) must be first adsorbed on the phlogopite particles in order to be later oxidized by TCE. The morphology of these precipitates differ significantly from those particles formed upon Hg(II), or As(V), oxidation of Fe(II). In the case of TCE, elongated particles (50 nm long) with an aspect ratio of approximately 2.5 are formed after 5 days reaction time (Fig. 8 and Table 1).

Furthermore, the elongated precipitates are distributed randomly over the phlogopite (001) terraces, instead of being preferentially located on the clay edges. The morphologic difference between the elongated particles, formed upon TCE reduction, and the amorphous-like circular ferric particles, formed upon Fe(II) oxidation by As or Hg, could be due to electron transfer kinetics. Iron hydroxides formed from Fe(II) are known to be lepidocrocite at

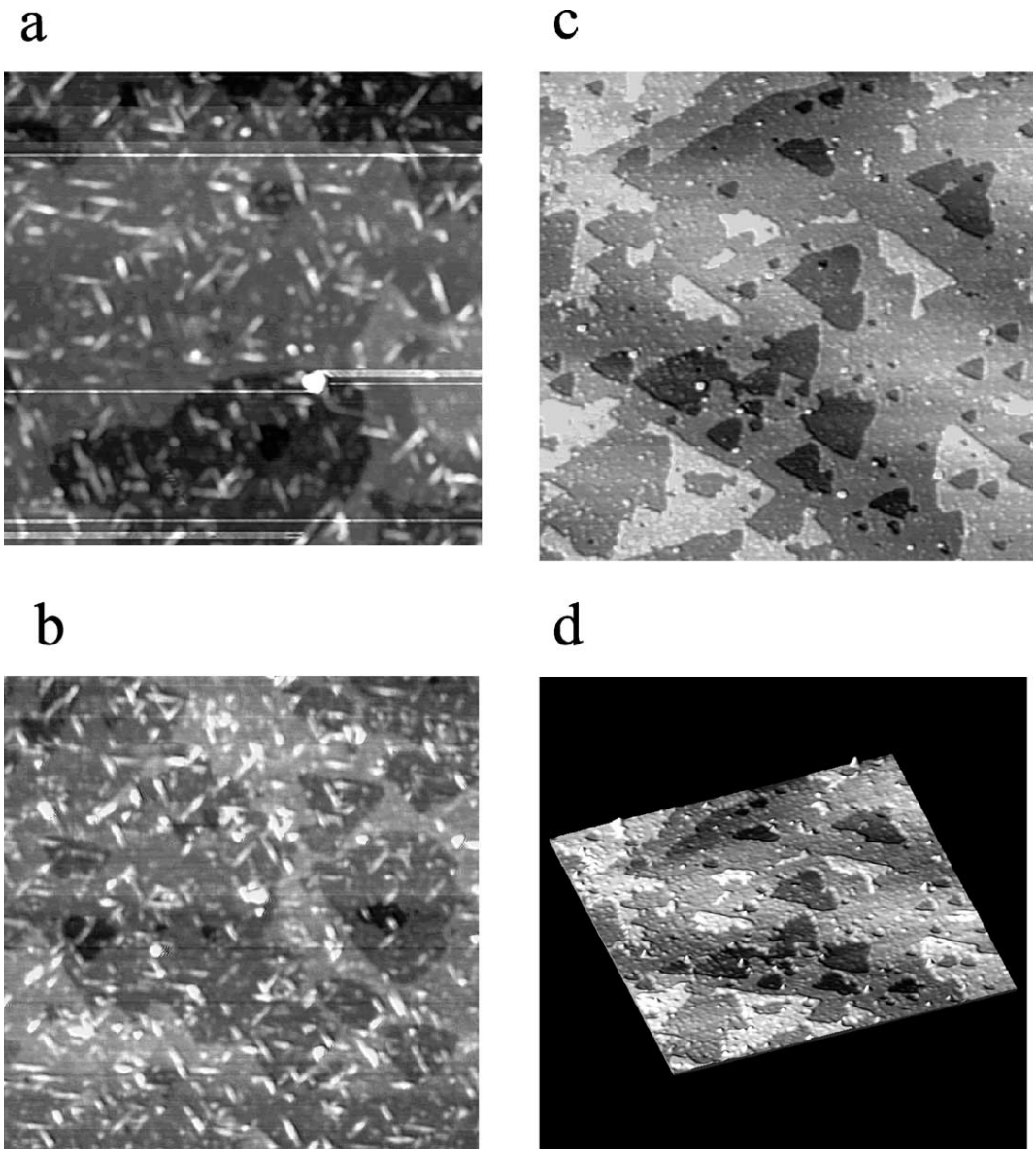

Fig. 7. In situ AFM Images of the phlogopite surface reacted with Fe(II) and TCE. Reaction time: 5 days. (a) and (b) were obtained in absence of background ionic medium, while (c) and (d) were obtained in 0.1 M NaCl background ionic medium.

intermediate oxidation rate, ferrihydrite at fast oxidation rate or goethite at slow oxidation rates (Cornell and Schwertmann, 1996). Arsenic(V) and mercury(II) are expected to be specifically adsorbed on clay edge surface sites (Sarkar et al., 2000; Xu et al., 1988), together with Fe(II). A fast inner-sphere electron transfer could then occur and lead to a ferrihydrite precipitation process. The presence of silicic acid, released upon dissolution of phlogopite etch pits, would further inhibit Fe(III) polymerisation (Doelsch et al., 2000) and lead to the preferential precipitation of small ferrihydrite particles (Karim, 1984). TCE on the contrary has been reported not to form inner sphere complexes, neither with Fe(II) nor with mineral surface

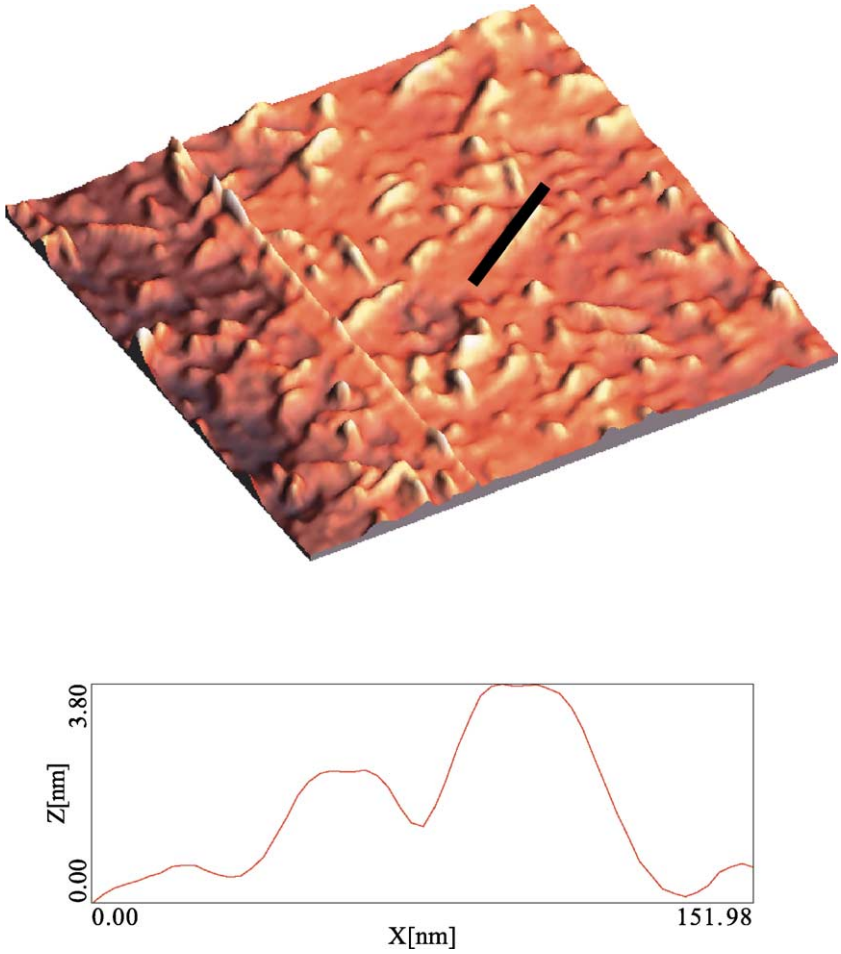

Fig. 8. Zoom (a) and transect (b) of the AFM image of the Fe(II)-phlogopite surface reacted 5 days with TCE.

functional groups. As in the case of nitrobenzene (Charlet et al., 1998b; Schultz and Grundl, 2000), this could lead to slow redox kinetics, and thus to the heterogeneous formation of goethite-like surface precipitates (Ramsden and Mate, 1998).

The orientation of the elongated needles sitting on the clay (001) terraces is not random. Three distinct preferential orientations can be easily recognized (Fig. 6a,b), which coincide with the crystallographic direction of periodic bond chains in the phlogopite structure, as indicated in Fig. 3. At this stage, it is not clear whether the preferential orientation of the Fe precipitates is a consequence of an epitaxial overgrowth. However, the Fe hydroxide particles were not wiped away during the contact mode AFM imaging procedure, which indicates that the precipitates are tightly bound to the phlogopite basal surface.

5. Discussion

5.1. Mechanisms of adsorption on phlogopite

Adsorption of cations on phyllosilicates results from the formation of two different types of surface

complexes, with two different surface functional groups. First, heteroionic cationic substitutions impart to phyllosilicates a permanent negative structural charge, which is compensated by the adsorption of cations on basal planes. In natural phlogopite, these cations are K^+ ions that may have lost part of their hydration shell. However, the acid treatment imposed on our phlogopite sample upon etching must have released a large part of these potassium ions, which were replaced first by protons, and second by Na^+, introduced together with the MOPS pH buffer. Sodium ion forms outer sphere (OS) surface complexes (Sposito et al., 1999) and are easily exchanged with solute ions (e.g. $Fe(H_20)_6^{2+}$) by varying the cationic composition of the solution. In this adsorption mechanism, the sorbate cation (Na^+, Fe^{2+}) is held in the vicinity of the sorbent surface without loosing its hydration shell. In such a complex, ferrous ion is not expected to undergo hydrolysis at pH 7.5 (pK_1=10.1 for the first Fe(II) first hydrolysis; Stumm and Sulzberger, 1992). The rate of electron transfer between $Fe(H_20)_6^{2+}$ and an oxidant species will then be slow with neutral species (e.g. $Hg(OH)_2^\circ(aq)$ or $O_2(g)$) and very slow for anionic species (e.g. $HA_sO_4^{2-}(aq)$), which are electrostatically repulsed from the negatively charged phlogopite surface.

Besides these cation exchange properties, phyllosilicates also possess pH-dependent sorption properties. Trioctahedral smectites (e.g. hectorite) and micas (e.g. phlogopite) are built of layers made by the condensation of one central magnesian octahedral sheets and two tetrahedral sheets. The pH-dependent sorption was inferred to take place at layer edges, where truncation of the bulk structure leads to the formation of oxygen dangling bonds. The edge surfaces and their broken bonds are characterized by a well-known tendency to form inner sphere complexes with protons and other cations (e.g. White and Zelazny, 1988; Zachara and McKinley, 1993; Charlet et al., 1993; Schlegel et al., 1999; Wanner et al., 1994). The formation of these inner sphere (IS) surface complexes involves the creation of chemical bonds between the sorbate and the surface oxygens of the sorbent (Cases et al., 2000). Surface cations of the sorbent thus enter the second coordination sphere of the sorbate. Thanks to polarized EXAFS spectroscopy, divalent cations (e.g. Co^{2+} and Zn^{2+}) were shown to form IS complexes with the edges of the hectorite platelets, in the prolongation of the octahedral sheet. The cation octahedra share one or several edges with structural octahedra and one or several corners with Si tetrahedra, like in a clay structure (Schlegel et al., 1999, 2000). Excess of divalent cations can lead to the formation of octahedral sheets parallel to the ab plane of hectorite crystallites, and if present, these polymers may incorporate Si to form clay minerals (Schlegel et al., 2001).

5.2. Reduction mechanism

Divalent cation sorption on silica and (hydr)oxides lead to their enhanced hydrolysis, compared to solution (Schindler, 1991). Similarly, sorption of Fe(II) on the edges of phlogopite platelets, i.e. on the walls of etch pits, is expected to lead to the formation of reactive $>SOFe^{II}(OH)_i^{1-i}$ with surface species (S=Mg or Si and i=0 or 1). Hydroxyl groups will in turn facilitate the electron transfer to the oxidant species, as the OH^- ligands donate electron density to Fe(II) through both σ and π systems. A kinetic mechanism consistent with our results involves: (i) rapid adsorption of Fe(II) and formation of reactive $>SOFe^{II}(OH)_i^{1-i}$,(ii) reduction of ox (with ox=Hg(II) or As(V)) by $>SOFe^{II}(OH)_i^{1-i}$ through formation of an activated surface complex or an outer sphere complex, and (iii) precipitation of $Fe(OH)_3(s)$.

We shall first discuss in detail the reduction of Hg(II) by surface Fe(II). The experimental results obtained in the present study (Fig. 2a) show the formation of gaseous mercury immediately after Hg(II) addition. This suggests that the principal "supply" of mercury is dissolved mercury present in the aqueous layer in the vicinity of surface rather than sorbed mercury. Thermodynamic calculations demonstrate the dominant solution species at pH >4 to be $Hg(OH)_2^\circ$ in the absence of chloride ion. Production of $Hg^\circ(g)$ involves formation of an activated "outer sphere" complex between $>SOFe^{II}(OH)_i^{1-i}$ and $Hg(OH)_2^\circ$, the OH^- groups mediating the hydrogen bridging through which electron transfer occurs. The proposed mechanism includes the following steps:

$$>SOH^\circ + Fe^{2+} + iH_2O \xleftrightarrow{K_1} >SOFe^{II}(OH)_i^{1-i} + (i+1)H^+ \quad \text{(i)}$$

$$2 > \mathrm{SOFe^{II}(OH)}_i^{1-i} + \mathrm{Hg(OH)}_2^0 \underset{k_{-2}}{\overset{k_2}{\rightleftharpoons}} [> \mathrm{SOFe^{II}(OH)}_i \cdots \mathrm{HOHg^{II}OH} \cdots \times \mathrm{(HO)}_i\mathrm{Fe^{II}OS} <] \quad \text{(ii)}$$

$$[> \mathrm{SOFe^{II}(OH)}_i \cdots \mathrm{HOHg^{II}OH} \cdots \mathrm{(HO)}_i\mathrm{Fe^{II}OS} <] \xrightarrow{k_3} 2 > \mathrm{SOFe^{III}(OH)}_{1+i}^{1-i} + \mathrm{Hg}^\circ \quad \text{(iii)}$$

$$> \mathrm{SOFe^{III}(OH)}_{1+i}^{1-i} + (2-i)\mathrm{H_2O} \xrightarrow{k_4} > \mathrm{SOH}^\circ + \mathrm{Fe(OH)}_{3(s)} + (1-i)\mathrm{H}^+ \quad \text{(iv)}$$

where K_1 is an intrinsic equilibrium constant; k_2, k_{-2}, k_3 and k_4 are rate constants. k_2 corresponds to the formation of precursor complexes, k_{-2} relates to the inverse rate, k_3 is the Hg° rate formation constant out of the transition complex and k_4 corresponds to the formation of a new $\mathrm{Fe^{III}(OH)_{3(s)}}$ solid phase at the surface of phlogopite.

From the model given in Eqs. (i)–(iv), a complete rate-law expression, more complex than Eq. (4), is derived. After applying the steady-state principle to the formation of the precursor complex and suggesting that $k_{-2}k_3$ (Cervini-Silva et al., 2000) and that $C_{\mathrm{Hg^{2+}}} = C_{\mathrm{Hg(OH)_2^\circ}}$, the rate-law expression is given by

$$\frac{\mathrm{d}C_{\mathrm{Hg^{2+}}}}{\mathrm{d}t} = -\frac{k_2 K_1^2 C_{0>\mathrm{SOH}^\circ}^2 C_{\mathrm{Fe^{2+}}}^2}{C_{\mathrm{H^+}}^{2(i+1)}\left(1+\frac{K_1 C_{\mathrm{Fe^{2+}}}}{C_{H^+}^{i+1}}\right)^2} C_{\mathrm{Hg^{2+}}} \quad (5)$$

where $C_{0>\mathrm{SOH}}$ is a total concentration of surface sites. For our experimental conditions, i.e. at pH=7.5 and at an initial $\mathrm{Fe^{2+}}$ concentration, $C_{\mathrm{Fe^{2+}}}$ equal to 10 M, the term $(K_1 C_{\mathrm{Fe^{2+}}})/(C_{\mathrm{H^+}}^2)$ is smaller than 1 when $K_1 < 10^{-10}$. This value of the order of intrinsic equilibrium constants measured for the surface complexation of Fe(II) with other mineral surfaces (Zhang et al., 1992; Liger et al., 1999).

As the initial concentration of Fe(II) (10 μM) is much greater than the initial Hg(II) concentration (50 pM), the speciation of >SOH°, Fe(II) and $>\mathrm{SOFe^{II}(OH)}_i^{1-i}$ is expected not to vary much within the course of Hg° formation and Eq. (6) can be rewritten as a pseudo-first-order reaction with respect to Hg(II), with an observed rate constant (Eq. (4)):

$$k_{\mathrm{obs}} = \frac{k_2 K_1^2 C_{0>\mathrm{SOH}^\circ}^2 C_{\mathrm{Fe^{2+}}}^2}{C_{\mathrm{H^+}}^{2(i+1)}} = k_2 \frac{C_{0>\mathrm{SOH}^\circ}^2}{C_{>\mathrm{SOH}^\circ \mathrm{eq}}^2} C_{>\mathrm{SOFe^{II}(OH)}_i^{1-i}}^2 \quad (6)$$

It follows that the formation of the precursor complex is a rate-limiting step and that k_{obs} depends on the surface speciation of Fe(II) and on the concentration of $>\mathrm{SOFe^{II}(OH)}_i^{1-i}$ surface complexes. The variability of k_{obs} due to changes in abundance of hydroxo surface complex $>\mathrm{SOFe^{II}OH}^\circ$ has been documented for the reduction of inorganic compounds (U(VI), Liger et al., 1999) and organic species (4-chloronitrobenzene) (Charlet et al., 1998b).

The same oxidation mechanism is expected to apply to the two other oxidants, namely to $\mathrm{HA_sO_4^{2-}}$ and TCE. However, the type of $>\mathrm{SOH}^0$ surface site involved in these reactions may vary. Oxyanions, such as arsenate, are repelled from the structural negative charge bearing phlogopite basal plane, but may form, as for chromate, inner sphere complexes with mica book edges, as shown by XPS spectroscopy, and, when micas contain structural Fe(II) books, to enhance this way the Fe(II)–Cr(VI) electron transfer (Ilton and Veblen, 1994). Furthermore, arsenate has been shown by EXAFS spectroscopy to form with $>\mathrm{Fe^{III}OH}$ surface sites a bidentate mononuclear surface complex (Manceau, 1995). In the present case, $\mathrm{HA_sO_4^{2-}}$ is expected to form in Eq. (ii) a $[>\mathrm{SOFe^{II}}]_2\mathrm{As^{V}O_3^{2-}}$ activated surface complex. Eq. (iii) would lead to a mixed As(III)–As(V) coprecipitate with $\mathrm{Fe(OH)_{3(s)}}$. Similar mixed coprecipitates have been observed in the reduction of U(VI) by surface Fe(II) (Liger, 1996; Liger et al., 1999).

The TCE case differs from the Hg(II) and As(V) cases in as much as TCE is a neutral hydrophobic species. The clay surface exhibits hydrophilic properties for molecules whose adsorption does not lead to the removal of the charge-compensating cations, but exhibits hydrophobic properties for molecules that replace the charge-compensating cations, since the siloxane layer—which, in the absence of charge

compensating cations, is characterized exclusively by charge—satisfied extremely stable siloxane bonds (White and Zelazny, 1988; Staunton and Quiquampoix, 1994; Sposito et al., 1999). Cations with high hydration enthalpy, such as Fe^{2+}, are expected upon adsorption in the interlayer domain to remain fully hydrated. Thus, no enhancement of electron transfer via hydrolysis is expected for these cations. However, the pre-etching of phlogopite surfaces with HF may have created zones of mechanical weakness within micas that have been often shown to run parallel to the preferred growth faces (Bloss et al., 1959; Klein and Hurlbut, 1993).

Rufe and Hochella (1999) and Bosbach et al. (2000) recently examined with in situ AFM the dissolution behavior of phlogopite etch pits and hectorite platelets, respectively, in HCl solutions. The phlogopite etch pits and hectorite dissolution features were essentially euhedral along the preferred growth faces (Fig. 3). Since crystal growth is approximated as the formation of strong bonds between growth units of stoichiometric composition (Grim and Güven, 1978), and since growth faces are observed to lie parallel to one or more continuous chains of strong bonds within the crystal structure, called Periodic Bond Chains (PBCs), the dissolution of phlogopite must be initiated by precursors in which the basal plane siloxane bonds are weakened along PBCs. Grim and Güven (1978) and Hartman (1982) showed that the PBCs in phyllosilicates are along the <110> and <100> directions, so that ''pseudohexagonal'' stepped (110), (010) and (110) edge faces are predicted to be the dominant dissolution (Fig. 3). Surface oxygen atoms at these weakened sites may complex Fe(II) and polarize surrounding water molecules, which will in turn be bridging, in an outer sphere complex, the surface Fe(II) with TCE. Similarly, H_2O molecules mediating in an outer sphere complex the hydrogen bridge between Si–O basal groups and an organic molecule have been shown to promote dehydrochlorination reaction, e.g. that of pentachloroethane (5CA) by clay structural Fe(II) (Cervini-Silva et al., 2000). In our case, a hydrogen bridge is expected to be formed between TCE and Fe(II) complexed with free coordination sites located on the siloxane basal plane along PCB directions. These surface sites were not active for the two other oxidants which co-adsorb, and readily react, with Fe(II) on step surface sites. Surface atoms present at the weakened sites along PCB directions are characterized by a ligand sphere that differs from both that in the basal plane siloxane plane bulk, and that on the etch pits.

5.3. Environmental significance

The present experiments have shown that solid phases, i.e. mineral surfaces, have a strong influence on the reductive transformation of some priority pollutants. The kinetic study of this and two accompanying papers on the pH dependence of Hg reduction in the presence of synthetic and natural particles (Peretyashko et al., in preparation (a), in preparation (b)) help us to assess the redox behavior of mercury in natural environments. For example, in eutrophic lakes (Peretyashko et al., in preparation (b)) or hydromorphic soils (Peretyashko et al., in preparation (c)), surface reaction can be expected to dominate, whereas biotic Hg reduction will likely occur in oxic environments (Mason et al., 1995).

Reduction of As(V) and TCE, which are both frequent groundwater contaminants (McArthur et al., 2000; Christensen et al., 1994), lead to their natural attenuation and to hydrous ferric oxide reactions products localized in different structural features of the etched phlogopite/water interface. This leads to insights on their respective reduction mechanisms. As(V) is likely, like Cr(VI), to form inner sphere surface complexes at the edges and etch pits walls of micas particles (Ilton and Veblen, 1994; Xu et al., 1988), and to react there with sorbed Fe(II). On the other hand, reduction of TCE by Fe(II) is likely to occur by outer sphere complex formation. It reacts with Fe sorbed on basal plane surface sites located along the weakened bonds between bond chains.

Detailed surface studies help to optimize the application of Fe(II)/mineral mixtures as reductants of pollutants in technical systems. In situ remediation of contaminated soil and water by addition of soluble Fe(II) salts may be a cheap alternative to pump and treat remediation or to permeable, reactive Fe° barriers that might become less reactive with time because of surface passivation. The relative reactivities of the different surface Fe(II) species towards the three contrasted species chosen for this study are possibly transferable to predict the reduction of a number of other compounds.

Finally, this study provides compelling evidence that the so-called surface coatings of clay particles frequently encountered in soils may not be formed by transfer to the surface of homogeneously formed Fe(III) hydroxides (Hendershot and Lavkulich, 1983), but rather as a product of the heterogeneous oxidative precipitation of iron by a variety of natural electron acceptors. Electron micrographs of kaolinite and goethite association indicate goethite particles to be either associated with kaolinite basal plane (Tandy et al., 1988), as in the case of our TCE experiment, or to be located on clay edges (Muller and Bocquier, 1986), as in the case of our Hg(II) and As(V) experiments.

6. Conclusions

Our results confirm that Fe oxide coatings, often found in soil and aquifer materials at the surface of sand and clay particles (Cornell and Schwertmann, 1996), may not result from the homogeneous precipitation of Fe(III), but rather from the enhancement by the mineral surface of the rate of ferrous iron oxidation by a variety of oxidants. The in situ results show that although iron oxyhydroxides may precipitate in solution, the tiny (roughly 25 nm in diameter) particles observed in the present study are closely associated with topographical steps, i.e. with broken edges of the clay crystal. Therefore, ferrous iron ions were sorbed and oxidized by Hg(II) and As(V) on surface edge sites. These results are consistent with macroscopic measurements and ex situ atomic force microscopy of Fe(II) reactions products with other oxidants at the surface of iron oxides (Weidler et al., 1998; Liger et al., 1999). Thus, some extrapolation to a broader range of mineral surfaces and oxidants seems warranted.

While this study and previous ones show that at least some As is sequestrated by the nucleation and precipitation of a ferric solid phase, there are some inherent limitations to the methods used in this study. For example, AFM was not capable of atomic scale resolution; hence, we could not rule out a coprecipitation of As(V) or As(III) within the ferric oxyhydroxides nanoparticles precipitated on the phlogopite edges. Likewise, AFM is a surface-sensitive method, so that we could not rule out the possibility of reaction between TCE and structural Fe(II), a reaction suggested by the nanoparticles lining up along crystallographic axis. Structure-sensitive and depth-sensitive measurements (i.e. X-ray absorption spectroscopy, and Mössbauer spectroscopy) are presently being obtained and will be presented in a future publication to address these issues. Nevertheless, the imaging of chemisorbed Fe(II) permits an interpretation of elementary steps in important catalytic reactions at an atomic level. This type of study should encourage surface science research further towards investigations into dynamic processes occurring on clay surfaces.

Acknowledgements

L.C. gratefully acknowledges partial support of this work by the program "Mercury in French Guyana" (CNRS-MATE-FEDER), the Indian-French Center for Advanced Research ("Geochemistry of Arsenic in Ganga River sediments" Project), and ADEME (V. Barbu scholarship). L.C. and D.B. acknowledge the Franco-German "Procope" project #9915, and T.P the support of a fellowship from the French Ministry for Foreign Affairs. **[EO]**

References

Appelo, C.A.J., Drijver, B., Hekkenberg, R., De Jonge, M., 2000. Modeling in situ iron removal from ground water. Ground Water 37, 811–817.

Bickmore, B.R., Hochella, M.F., Bosbach, D., Charlet, L., 1999a. Atomic force microscopic imaging of minutes particles in aqueous solutions. Microsc. Today 99 (9), 14–18.

Bickmore, B.R., Hochella, M.F., Bosbach, D., Charlet, L., 1999b. Methods for performing atomic force microscopy imaging of clay minerals in aqueous solutions. Clays Clay Miner. 47, 573–581.

Bickmore, B.R., Bosbach, D., Hochella Jr., M.F., Charlet, L., Rufe, E., 2001. In situ atomic force microscopy study of hectorite and nontronite dissolution: implications for phyllosilicate edge structures and dissolution mechanisms. Am. Mineral. 86, 411–423.

Bloom, N.S., Fitzgerald, W.F., 1988. Determination of volatile mercury species at the picogram level by low-temperature gas chromatography with cold-vapor atomic fluorescence detection. Anal. Chim. Acta 208, 151–161.

Bloss, F.D., Sherkarchi, E., Shell, H.R., 1959. Hardness of synthetic and natural micas. Am. Mineral. 44, 33–48.

Bosbach, D., Charlet, L., Bickmore, B., Hochella Jr., M.F., 2000. The dissolution of hectorite: in-situ, real-time observations using atomic force microscopy. Am. Mineral. 85, 1209–1216.

Buerge, I.J., Hug, S.J., 1999. Influence of mineral surfaces on chromium(VI) reduction by Fe(II). Environ. Sci. Technol. 33, 4285–4291.

Cases, J.M., Villiéras, F., Michot, L., 2000. Adsorption, exchange and retention phenomena at the solid–aqueous interface: 1. Influence of structural, textural and superficial properties of solids. C. R. Acad. Sci. Paris, Earth Planet. Sci. 331, 763–773.

Cervini-Silva, J., Wu, J., Stucki, J.W., Larson, R.A., 2000. Adsorption kinetics of pentachloroethane by iron-bearing smectites. Clays Clay Miner. 48 (1), 132–138.

Charlet, L., Schindler, P.W., Spadini, L., Furrer, G., Zysset, M., 1993. Cation adsorption on oxides and clays: the aluminum case. Aquat. Sci. 55, 291–303.

Charlet, L., Liger, E., Gerasimo, P., 1998a. Decontamination of TCE and uranium-rich waters by granular iron: role of sorbed Fe(II). J. Environ. Eng. 124, 25–30.

Charlet, L., Silvester, E.J., Liger, E., 1998b. N-compound reduction and actinide immobilisation in surficial fluids by Fe(II): the surface equivalent to $>Fe^{III}OFe^{II}OH^{\circ}$ degrees species as major reductant. Chem. Geol. 151, 85–93.

Christensen, T.H., Kjeldsen, P., Albrechtsen, H.J., Nielsen, P.H., Bjerg, P.L., Holm, P.E., 1994. Attenuation of landfill leachate pollutants in aquifers. Crit. Rev. Environ. Sci. Technol. 24 (4), 119–202.

Cornell, R.M., Schwertmann, U., 1996. The Iron Oxides VCH Verlag, Weinheim.

Cossa, D., Mason, P.P., Fitzgerald, W.F., 1994. Chemical speciation of mercury in a meromictic lake. In: Watras, C.J. (Ed.), Mercury Pollution, Integration and Synthesis. Lewis Publ., Boca Raton.

Cui, D., Eriksen, T.E., 1996. On the reduction of pertechnetate by ferrous iron in solution; influence of sorbed and precipitated Fe(II). Environ. Sci. Technol.

Davison, W., Grime, G.W., Morgan, J.A.W., Clarke, K., 1991. Distribution of dissolved iron in sediment pore waters at submillimeter resolution. Nature 352, 323–325.

Doelsch, E., Rose, J., Masion, A., Bottero, J.Y., Nahon, D., Bertsch, P.M., 2000. Speciation and crystal chemistry of iron(III) chloride hydrolyzed in the presence of SiO_4 ligands: 1. An FeK-edge EXAFS study. Langmuir 16 (10), 4726–4731.

Eggleston, C.M., Stumm, W., 1993. Scanning tunneling microscopy of Cr(III) chemisorbed on α-Fe_2O_3(001) surfaces from aqueous solution: direct observation of surface mobility and clustering. Geochim. Cosmochim. Acta 57, 4843–4850.

Environmental Protection Agency, 1997. Use of monitored natural attenuation at Superfund, RCRA Corrective Action, and underground storage tank sites. Directive 9200, 4-17P, Office of Solid Waste and Emergency Response, Washington DC, 32 pp.

Ernstsen, V., 1996. Reduction of nitrate by Fe^{2+} in clay minerals. Clays Clay Miner. 44, 599–608.

Grim, R.E., Güven, N., 1978. Bentonites. Geology, mineralogy, properties and uses. Dev. Sedimentol., 24. Elsevier, Amsterdam, Netherlands.

Hartman, P., 1982. On the growth of dolomite and kaolinite crystals. Neuese Jahrbuch für Mineralogie, Monatshefte, 84–92.

Hartman, P., 1983. Calculation of electrostatic bonding energy and lattice energy of polar phyllosilicates: kaolinite and chlorite. Clays Clay Miner. 31, 218–222.

Hendershot, W.H., Lavkulich, L.M., 1983. Effect of sequioxide coating on surface charge of standard mineral and soil samples. Soil Sci. Soc. Am. J. 47, 1252–1260.

Heron, G., Christensen, T.H., 1995. Impact of sediment bound iron on redox buffering in a landfill leachate polluted aquifer (Vejen, Denmark). Environ. Sci. Technol. 29 (1), 187–192.

Hug, S.J., Johnson, A., Friedl, G., Lichtensteiger, T., Belevi, H., Sturm, M., 1997. Characterization of environmental solid and surfaces. Chimia 51, 884–892.

Ilton, E.S., Veblen, D.S.R., 1994. Chromium sorption by phlogopite and biotite in acidic solutions at 25 °C: insights from X-ray photoelectron spectroscopy and electron microscopy. Geochim. Cosmochim. Acta 58 (13), 2777–2788.

Karim, Z., 1984. Characteristics of ferrihydrites formed by oxidation of $FeCl_2$ solutions containing different amounts of silica. Clays Clay Miner. 32 (3), 181–184.

Klausen, J., Tröber, P.T., Haderlein, S.B., Schwarzenbach, R.P., 1995. Reduction of substituted nitrobenzenes by Fe(II) in aqueous mineral suspensions. Environ. Sci. Technol. 29, 2396–2404.

Klein, C., Hurlbut, C.S., 1993. Manual of Mineralogy, 21st ed. Wiley, New York 681 pp.

Liger, E., 1996. Role catalytique des oxyhydroxydes de Fe(III): réduction de U(VI) par le Fe(II) adsorbé. PhD diss. Univ. Grenoble, France.

Liger, E., Charlet, L., Van Cappellen, P., 1999. Surface catalysis of uranium (VI) reduction by iron(II). Geochim. Cosmochim. Acta 19/20, 2939–2956.

Luther, G.W., 1990. The frontier-molecular-orbital theory approach in geochemical processes. In: Stumm, W. (Ed.), Aquatic Chemical Kinetics. Wiley-Interscience, New York, pp. 173–198.

Manceau, A., 1995. The mechanism of anion adsorption on Fe oxides: evidence for the bonding of arsenate tetrahedra on free $Fe(O,OH)_6$ edges. Geochim. Cosmochim. Acta 59, 3647–3653.

Mason, R.P., Morel, F.M.M., Hemond, H.F., 1995. The role of microorganisms in elemental mercury formation in natural waters. Water Air Soil Pollut. 80, 775–787.

McArthur, J.M., Ravenscroft, P., Safiullah, S., Thirlwall, M.F., 2000. Arsenic in groundwater: testing pollution mechanisms for sedimentary aquifers in Bangladesh. Water Resour. Res. 37 (1), 109–117.

Muller, J.P., Bocquier, G., 1986. Dissolution of kaolinites and accumulation of iron oxides in lateritic-ferruginous nodules: mineralogical and microstructural transformations. Geoderma 37, 113–136.

Myrreni, S.C.B., Tokunaga, T.K., Brown Jr., G.E., 1997. Abiotic selenium redox transformations in the presence of Fe(II, III) oxides. Science 278, 1106–1111.

Orth, W.C., Gillham, R.W., 1996. Dechlorination of trichloroethene in aqueous solution using Fe(0). Environ. Sci. Technol. 30, 66–71.

Ottley, C.J., Davison, W., Edmunds, W.M., 1997. Geochim. Cosmochim. Acta 61, 1819–1828.

Peretyashko, T., Charlet, L., Cossa, D., 2003a. Production of gaseous mercury in anoxic environments: reservoir Petit Saut, French Guyana (in preparation).

Peretyashko, T., Charlet, L., Cossa, D., Kazimirov, V., 2003b.

Mechanism of Hg° production by heterogeneous oxidation of Fe(II) (in preparation).
Peretyashko, T., Charlet, L., Grimaldi, M., 2003c. Production of gaseous mercury in flooded hydromorphic soils (in preparation).
Plaschke, M., Römer, J., Klenze, R., Kim, J.I., 1999. In situ AFM study of sorbed humic acid colloids at different pH. Colloids Surf., A 160, 269–279.
Ramsden, J.J., Mate, M., 1998. Kinetics of monolayer particle deposition. J. Chem. Soc., Faraday Trans. 94, 783–788.
Rufe, E., Hochella Jr., M.F., 1999. Quantitative assessment of reactive surface area of phlogopite dissolution during acid dissolution. Science 285, 874–876.
Sarkar, D., Essington, M.E., Misra, K.C., 2000. Adsorption of mercury(II) by kaolinite. Soil Sci. Soc. Am. 64, 1968–1975.
Schindler, P.W., 1991. A solution chemists view of surface chemistry. Pure Appl. Chem. 63, 1697–1704.
Schlegel, M.L., Manceau, A., Chateigner, D., Charlet, L., 1999. Sorption of metal ions on clay minerals: I. Polarized EXAFS evidence for the adsorption of Co on the edges of hectorite particles. J. Colloid Interface Sci. 215, 140–158.
Schlegel, M.L., Charlet, L., Manceau, A., 2000. Sorption of metal ions on clay minerals. II. mechanism of Co sorption on hectorite at high and low ionic strength, and impact on the sorbent stability. J. Colloid Interface Sci. 220, 392–405.
Schlegel, M.L., Manceau, A., Charlet, L., Hazemann, J.L., 2001. Adsorption mechanism of Zn on hectorite as a function of time, pH and ionic strength. Am. J. Sci. 301, 755–772.
Schultz, C.A., Grundl, T.J., 2000. pH dependence on reduction rate of 4-Cl-Nitrobenzene by Fe(II)/montmorillonite systems. Environ. Sci. Technol. 34, 3641–3648.
Schwertmann, U., Pfab, G., 1994. Structural vanadium in synthetic goethite. Geochim. Cosmochim. Acta 58 (20), 4349–4352.
Sorensen, J., Thorling, L., 1991. Stimulation of lepidocrocite (γ-FeOOH) of Fe(II)-dependent nitrite reduction. Geochim. Cosmochim. Acta 55, 1289–1294.
Sposito, G., Skipper, N.T., Sutton, R., Park, S.-H., Soper, A., Greathouse, J.A., 1999. Surface geochemistry of the clay minerals. Proc. Natl. Acad. Sci. 96, 3358–3364.
Staunton, S., Quiquampoix, H., 1994. Adsorption and conformation of bovine serum albumin on montmorillonite: modification of the balance between hydrophobic and electrostatic interactions by protein methylation and pH variation. J. Colloid Interface Sci. 166, 89–94.
Stumm, W., Sulzberger, B., 1992. The cycling of iron in natural environments; considerations based on laboratory studies of heterogeneous redox processes. Geochim. Cosmochim. Acta 56, 3233.
Tandy, J.C., Grimaldi, M., Grimaldi, C., Tessier, D., 1988. Mineralogical and textural changes in French Guyana oxisols and their relation with microaggregation. Developments in Soil Science. Soil micromorphology: a basic and applied science. Proc. Congress Soil Micromorphology, San Antonio Texas. Elsevier Publ. 19, 191–198.
Tamura, H., Kawamura, S., Nagayama, M., 1980. Acceleration on the oxidation of Fe^{2+} by Fe(III) oxyhydroxides. Corros. Sci. 20, 963–971.
Vanek, V., 1990. In situ treatment of iron-rich groundwater by the addition of nitrate. Rep. Lunds Universitet, 33 pp.
Wanner, H., Albinsson, Y., Karnland, O., Wieland, E., Wersin, P., Charlet, L., 1994. The acid base chemistry of montmorillonite. Radiochimica 66/67, 157–162.
Weidler, P.G., Hug, S.J., Wetche, T.P., Hiemstra, T., 1998. Determination of growth rates of (100) and (110) faces of synthetic goethite by scanning force microscopy. Geochim. Cosmochim. Acta 62, 3407–3412.
White, G.N., Zelazny, L.W., 1988. Analysis and implication of the edge structure of dioctaedral phylosilicates. Clays Clay Miner. 36 (2), 141–146.
Xu, H., Allard, B., Grimvall, A., 1988. Influence of pH and organic substance on the adsorption of As(V) on geological materials.
Zachara, J.M., McKinley, J.P., 1993. Influence of hydrolysis on the sorption of metal cations by smectites: importance of edge coordination reactions. Aquat. Sci. 55 (4), 250–261.
Zhang, Y., Charlet, L., Schindler, P.W., 1992. Adsorption of protons, iron(II) and aluminum(III) on lepidocrocite. Colloids Surf. 63, 259–268.